

Article

Description of the New Eutectic Al-Ca-Cu System in the Aluminum Corner

Torgom K. Akopyan^{1,2,*}, Nikolay A. Belov¹, Nikolay V. Letyagin¹, Stanislav O. Cherkasov¹ and Xuan D. Nguen¹

¹ Department of Metal Forming, National University of Science and Technology MISiS, 4 Leninsky pr., Moscow 119049, Russia; nikolay-belov@yandex.ru (N.A.B.); n.v.letyagin@gmail.com (N.V.L.); ch3rkasov@gmail.com (S.O.C.); xuandiep0307@gmail.com (X.D.N.)

² Sector of Scientific Activity, Moscow Polytechnic University, 38, Bolshaya Semyonovskaya str., Moscow 107023, Russia

* Correspondence: nemiroffandtor@yandex.ru

Abstract: The structure of the new ternary eutectic Al-Ca-Cu system considered as a replacement for the ternary eutectic system Al-Ce-Cu widely used for additive manufacturing has been studied using experimental techniques. The liquidus projection of the Al-Ca-Cu system in the aluminum corner has been suggested based on experiential studies of the microstructure and phase composition of model alloys. The suggested structure of the diagram has two quasi-binary sections: (Al)-Al₂₇Ca₃Cu₇ and (Al)-Al₈CaCu₄ and three invariant eutectic transformations: L→(Al) + (Al,Cu)₄Ca + Al₂₇Ca₃Cu₇ (at 5.6 wt.% Ca, 4.5 wt.% Cu, 595 °C), L→(Al) + Al₂₇Ca₃Cu₇ + Al₈CaCu₄ (at 2.2 wt.% Ca, 13.5 wt.% Cu, 594 °C) and L→(Al) + Al₈CaCu₄ + Al₂Cu (at 0.5 wt.% Ca, 34 wt.% Cu, 544 °C). The limit solubility of copper in aluminum solid solution (Al) at 530 °C reaches ~5.1 wt.% in the ternary phase field (Al) + Al₈CaCu₄ + Al₂Cu and drops to ~2.4 wt.% in the (Al) + Al₈CaCu₄ + Al₂₇Ca₃Cu₇ ternary phase field. For the example of the model ternary hypoeutectic alloys with a predominant content of the eutectic (Al,Cu)₄Ca phase, it has been shown that the system is promising for designing new eutectic-type alloys with a natural composite structure.



Citation: Akopyan, T.K.; Belov, N.A.; Letyagin, N.V.; Cherkasov, S.O.; Nguen, X.D. Description of the New Eutectic Al-Ca-Cu System in the Aluminum Corner. *Metals* **2023**, *13*, 802. <https://doi.org/10.3390/met13040802>

Academic Editors: Petra Maier and Normen Fuchs

Received: 28 February 2023

Revised: 8 April 2023

Accepted: 16 April 2023

Published: 19 April 2023



Copyright: © 2023 by the authors. Licensee MDPI, Basel, Switzerland. This article is an open access article distributed under the terms and conditions of the Creative Commons Attribution (CC BY) license (<https://creativecommons.org/licenses/by/4.0/>).

Keywords: phase diagram; Al-Ca-Cu system; microstructure; intermetallics

1. Introduction

Al-Cu-based alloys are widely used in load-bearing applications at room and relatively high temperatures (up to 225 °C) due to their good strength-to-weight ratio and toughness after artificial aging [1–3]. However, the wide solidification range typical of these alloys leads to various casting defects such as hot-tearing, shrinkage, and microporosity [4]. In contrast, eutectic Al-Re based alloys (Re = rare earths) have excellent resistance to hot-tearing [5], and thus high casting manufacturability. Earlier studies revealed [6–8] that the addition of Re in Al-Cu based alloys allows one to increase the resistance to hot-tearing, thus improving the castability due to the formation of a eutectic structure. Moreover, Al-Cu-Re based alloys have a good combination of mechanical properties at room and elevated temperatures [8,9] and exhibit high processability for additive manufacturing (AM) techniques [10], such as selective laser melting. Indeed, the high cooling rates used for AM provide for the formation of nano-sized eutectic or quasi-eutectic structures (in hypereutectic alloys [11]) which in turn provide for the effective strengthening by the Orowan mechanism [12,13], for which dislocations bypass the intermetallic particles by looping around them. For example, new Al-9Cu-6Ce and Al-9Cu-6Ce-1Zr (wt.%) alloys obtained by laser powder bed fusion AM have an ultra-fine eutectic structure consisting of an aluminum matrix and a eutectic intermetallic phase identified as Al₈Cu₃Ce [14,15]. The structure formed provides for a high strength at room and elevated temperatures of up to 400 °C.

However, despite the described advantages of the Al-Cu-Ce alloys, their fundamental drawback is the necessity of adding high concentrations of the relatively expensive rare earth Ce. We believe that a calcium (Ca) additive can serve as an adequate replacement for rare earth metals. Indeed, calcium is a widespread, environmentally-friendly alkaline earth metal. Ca forms a eutectic-type system with aluminum and exhibits a very low solubility in Al (<0.01 at.%) [16], even after the severe plastic deformation [17] of the Al-Ca based alloy. According to numerous studies, as-cast [18–20] and wrought [17,21,22] Al-Ca-based alloys have a fine eutectic structure and a good combination of mechanical properties and manufacturability. The ternary Al-Ca-Cu system is also of interest, but it has been poorly studied [23,24]. It is well-known that information on the structure of phase diagrams is required for the informed design of new alloys. According to an earlier study [25], four intermetallic compounds, i.e., $(Al,Cu)_4Ca$, $Al_{27}Ca_3Cu_7$, Al_8CaCu_4 and Al_2Cu , can be in equilibrium with (Al) in the Al-Ca-Cu ternary system. The chemical composition and crystallographic structure of these compounds have recently been reported [25]. The presence of this many compounds in equilibrium with aluminum determines the very complex structure of this ternary diagram, and it is hardly possible to completely describe it in a single study. For comparison, the Al-Cu-Ce ternary system, where two phases ($Al_{11}Re_3$ and Al_8ReCu_4 [8,26]) are considered to be in equilibrium with aluminum, has been studied for the last decade, but nevertheless there is still controversy regarding its structure.

Thus, the aim of this work is to provide a first insight into the new system and to reveal the main features inherent in the structure of its phase diagram, and also to deliver sufficient information on the phase equilibria and transformations that determine the structure of the Al-Ca-Cu alloys upon solidification and high temperature annealing.

2. Materials and Methods

Several model alloys of the Al-Ca-Cu system (Table 1 and Figure 1) were chosen and prepared for studies. The alloys were prepared from 99.99% aluminum in a resistance furnace (GRAFICARBO) with a graphite crucible. Aluminum was placed in the crucible, and after its melting, copper in the form of pure metal (99.9 wt.% Cu) and calcium in the form of the binary Al-15%Ca master alloy were introduced into the melt. After the melting of the main components, the melt was held for 5–10 min to obtaining a homogeneous composition, and the metal was then cast into a $10 \times 20 \times 180$ mm graphite mold. The cooling rate in the mold was about 10 K/s. For achieving a close-to-equilibrium state at least at the beginning of the solidification, some alloys were remelted and slowly solidified in the furnace chamber at a cooling rate of about 0.02 K/s.

Table 1. Actual chemical composition of the experimental alloys.

| № | Designation | Actual Concentrations, wt.% | | |
|----|--------------|-----------------------------|------|------|
| | | Al | Ca | Cu |
| 1 | Al1.0Cu8.0Ca | balance | 8.8 | 1.6 |
| 2 | Al2.2Cu6.7Ca | balance | 6.6 | 2.5 |
| 3 | Al3.4Cu5.6Ca | balance | 5.6 | 3.6 |
| 4 | Al5.6Cu3.5Ca | balance | 3.9 | 6.6 |
| 5 | Al9.0Cu3.5Ca | balance | 3.5 | 9.0 |
| 6 | Al10Cu0.5Ca | balance | 0.35 | 9.0 |
| 7 | Al10Cu1.5Ca | balance | 1.2 | 9.0 |
| 8 | Al14Cu2.5Ca | balance | 2.5 | 14.0 |
| 9 | Al14Cu6.0Ca | balance | 6.5 | 13.0 |
| 10 | Al18Cu6.0Ca | balance | 6.0 | 15.0 |
| 11 | Al30Cu1.0Ca | balance | 1.0 | 27.0 |
| 12 | Al36Cu1.0Ca | balance | 1.5 | 35.0 |
| 13 | Al9.0Cu0.5Ca | balance | 0.4 | 8.2 |
| 14 | Al9.0Cu1.5Ca | balance | 0.8 | 8.5 |

Table 1. Cont.

| № | Designation | Actual Concentrations, wt.% | | |
|----|-------------|-----------------------------|-----|------|
| | | Al | Ca | Cu |
| 15 | Al14Cu1.0Ca | balance | 1.1 | 13.2 |
| 16 | Al14Cu7.0Ca | balance | 8.3 | 14.2 |
| 17 | Al3Ca0.5Cu | balance | 2.7 | 0.5 |
| 18 | Al3Ca1Cu | balance | 3.0 | 1.0 |

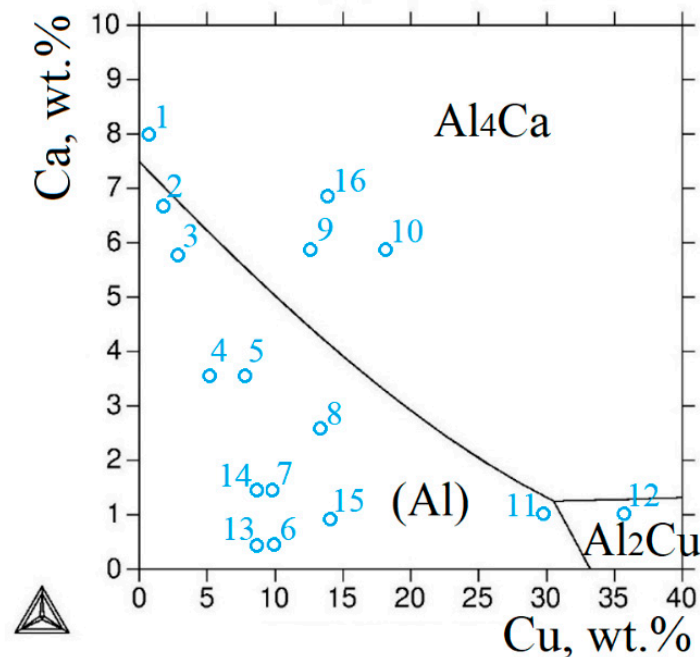


Figure 1. Composition of the chosen experimental alloys marked on the liquidus projection of the Al-Ca-Cu system calculated using Thermo-Calc software.

The Al10Cu0.5Ca and Al10Cu1.5Ca alloys were subjected to homogenization annealing at 530 °C for 10 h. Al3Ca0.5Cu and Al3Ca1Cu ingots without preliminary annealing were subjected to hot rolling (at 300 °C) to 2 mm sheet samples with an 80% reduction. The ingots were heat treated in muffle electric furnaces with a temperature control accuracy of ~3 K.

The microstructure was examined by means of scanning electron microscopy (SEM, TESCAN VEGA 3) and electron microprobe analysis (EMPA, OXFORD AZtec). The samples were polished for the studies. The metallographic samples were ground with SiC abrasive paper and polished with 1 µm diamond suspension. A solution of 1% hydrogen fluoride (HF) water was used for etching.

X-ray diffraction (XRD) data were collected using CoK α radiation and treated with a software package [27]. The specimens for the X-ray diffraction study were polished specimens cut from part of the ingots.

The solidification pattern of some alloys was studied by means of experimental cooling curves recorded using an AKTAKOM-2006 registering unit (Lutron Electronic Enterprise Co., Ltd., Taipei City, Taiwan) and chromel–alumel thermocouples.

The Vickers hardness (Hv) was measured using a DUROLINE MH-6 setup (METKON Instruments) with a load of 1 kg and a dwell time of 10 s. Room-temperature tensile tests of as-processed wire specimens were conducted on a Zwick Z250 universal testing machine (the loading rate was 10 mm/min). The flat proportional samples without grippers and with a size of 110 × 10 × 2 mm were used for the tensile tests.

In order to facilitate the preliminary analysis of the ternary system, a thermodynamic calculation of the liquidus projection of the Al-Ca-Cu system (Figure 1) was carried out using the Thermo-Calc software and the TTAL5 database [28]. It can be seen that the calculation suggests the existence of two intermetallic compounds: Al_4Ca and Al_2Cu , in equilibrium with aluminum and one invariant eutectic phase transformation $\text{L} \rightarrow (\text{Al}) + \text{Al}_4\text{Ca} + \text{Al}_2\text{Cu}$ in this corner.

3. Results and Discussion

3.1. Liquidus Projection

Experimental plotting of the liquidus projection in the system requires that the primary crystallization areas of the phases be identified. According to earlier data [25] and the experimental results of this study, three intermetallic Ca-containing phases, i.e., $(\text{Al,Cu})_4\text{Ca}$, $\text{Al}_{27}\text{Ca}_3\text{Cu}_7$ and Al_8CaCu_4 , can be in equilibrium with the aluminum solid solution (Al). In order to reveal the primary crystallization areas for each of the phases, the structure of some alloys pertaining to the respective areas was studied in detail. The primary crystallization areas were identified by the type of primary crystals observed in the structure.

Hypereutectic alloys were chosen for identifying the primary crystallization area of the phases. In the Al1.0Cu8.0Ca alloy, the primary crystals observed have a typical acicular structure, and according to spectral analysis for rapidly and slowly cooled alloys (Table 2), these crystals are the $(\text{Al,Cu})_4\text{Ca}$ phase. According to [25], the $(\text{Al,Cu})_4\text{Ca}$ phase is a solid solution based on the Al_4Ca phase with dissolved Cu atoms substituting Al. The primary crystals form against the fine eutectic background in the rapidly cooled alloy (Figure 2a). Slow cooling leads to the coarsening of the eutectic which, however, still remains relatively fine (Figure 2b). The Al2.2Cu6.7Ca alloy containing less Ca and more Cu also has a hypereutectic structure with less elongated and generally finer primary crystals (Figure 2c) which can also be clearly identified as the $(\text{Al,Cu})_4\text{Ca}$ [25] phase (Table 2). The eutectic looks uniform but much coarser. In the Al14Cu6.0Ca alloy with an excess of copper, a small fraction of another type of coarse crystals bright in appearance and having a compact spherical shape are observed along with the primary $(\text{Al,Cu})_4\text{Ca}$ phase crystals (Figure 2e). According to the EMPA data (Table 2), the solubility of copper in the $(\text{Al,Cu})_4\text{Ca}$ phase is the highest compared to that observed for the above-mentioned alloys. EMPA also revealed the chemical composition of the second type of crystals observed. Their phase is described by the formula $\text{Al}_{27}\text{Ca}_3\text{Cu}_7$ [25]. After the slow solidification of the Al14Cu6.0Ca alloy (Figure 2f), only $(\text{Al,Cu})_4\text{Ca}$ phase primary crystals are observed (marked by arrow). The latter fact suggests that the Al14Cu6.0Ca alloy pertains to the $(\text{Al,Cu})_4\text{Ca}$ phase primary field but is close to the $(\text{Al,Cu})_4\text{Ca}/\text{Al}_{27}\text{Ca}_3\text{Cu}_7$ boundary.

Table 2. Chemical composition of the phases detected in the alloys obtained at various cooling rates (Vs) upon solidification.

| Alloy | Vs, K/s | Chemical Composition, at.% | | | Phase Identification |
|--------------|---------|----------------------------|------|------|--|
| | | Al | Ca | Cu | |
| Al1.0Cu8.0Ca | 10 | balance | 19.6 | 2.0 | $(\text{Al,Cu})_4\text{Ca}$ |
| | 0.02 | balance | 19.3 | 2.1 | $(\text{Al,Cu})_4\text{Ca}$ |
| Al2.2Cu6.7Ca | 10 | balance | 19.3 | 3.3 | $(\text{Al,Cu})_4\text{Ca}$ |
| | 0.02 | balance | 19.0 | 3.8 | $(\text{Al,Cu})_4\text{Ca}$ |
| Al14Cu6.0Ca | 10 | balance | 19.0 | 8.0 | $(\text{Al,Cu})_4\text{Ca}$ |
| | | balance | 8.0 | 19.0 | $\text{Al}_{27}\text{Ca}_3\text{Cu}_7$ |
| | 0.02 | balance | 19.0 | 8.0 | $(\text{Al,Cu})_4\text{Ca}$ |
| | | balance | 8.0 | 19.0 | $\text{Al}_{27}\text{Ca}_3\text{Cu}_7$ |
| Al18Cu6.0Ca | 10 | balance | 19.2 | 8.3 | $(\text{Al,Cu})_4\text{Ca}$ |
| | 0.02 | balance | 7.9 | 18.9 | $\text{Al}_{27}\text{Ca}_3\text{Cu}_7$ |
| | | balance | 8.0 | 20.0 | $\text{Al}_{27}\text{Ca}_3\text{Cu}_7$ |

Table 2. Cont.

| Alloy | Vs, K/s | Chemical Composition, at.% | | | Phase Identification |
|--------------|---------|----------------------------|------|------|--|
| | | Al | Ca | Cu | |
| Al14Cu2.5Ca | 10 | balance | 8.0 | 20.0 | Al ₂₇ Ca ₃ Cu ₇ |
| | 0.02 | balance | 8.0 | 20.0 | Al ₂₇ Ca ₃ Cu ₇ |
| Al30Cu1.0Ca | 10 | balance | 6.6 | 30.1 | Al ₈ CaCu ₄ |
| | | | | | |
| Al36Cu1.0Ca | 10 | balance | 6.0 | 30.5 | Al ₈ CaCu ₄ |
| | 0.02 | balance | 7.8 | 33 | Al ₈ CaCu ₄ |
| Al3.4Cu5.6Ca | 0.02 | balance | 19.3 | 6.5 | (Al,Cu) ₄ Ca |
| | | | | | |
| Al5.6Cu3.5Ca | 0.02 | balance | - | 2.0 | (Al) |
| | | balance | 19.1 | 7.6 | (Al,Cu) ₄ Ca |
| | | balance | 7.8 | 17.6 | Al ₂₇ Ca ₃ Cu ₇ |
| Al9.0Cu3.5Ca | 0.02 | balance | - | 1.8 | (Al) |
| | | balance | 19.7 | 8.1 | (Al,Cu) ₄ Ca |
| | | balance | 7.4 | 18.2 | Al ₂₇ Ca ₃ Cu ₇ |

The Al14Cu2.5Ca and Al18Cu6.0Ca alloys were analyzed in order to clarify the boundaries of the primary crystallization area of the Al₂₇Ca₃Cu₇ compound. For the Al18Cu6.0Ca alloy, two types of coarse primary crystals are also observed (Figure 3a). The bright faceted crystals in Figure 3a are identified as the Al₂₇Ca₃Cu₇ phase, whose chemical composition perfectly matches that of the crystals in the Al14Cu6.0Ca alloy considered above. The second type of crystals, which are grey and elongated, are the (Al,Cu)₄Ca phase. The XRD data for this alloy (Figure 4) confirmed its phase composition consisting of both of the extra phases. However, after slow solidification (Figure 3b), only Al₂₇Ca₃Cu₇ phase primary crystals are observed. The latter fact confirms that the alloy pertains to the primary crystallization area of the Al₂₇Ca₃Cu₇ phase, but is close to the (Al,Cu)₄Ca/Al₂₇Ca₃Cu₇ boundary. After accelerated cooling, the Al14Cu2.5Ca alloy has a near-eutectic structure (Figure 3c) with lone Al₂₇Ca₃Cu₇ phase primary crystals. The presence of those crystals in the structure was also confirmed by XRD analysis (Figure 4). Along the Al₂₇Ca₃Cu₇ phase crystals, the patterns typical of the Al₈CaCu₄ phase [25] were also observed. After slow solidification, the alloy has a hypoeutectic structure (Figure 3d) with a high eutectic fraction. These facts demonstrate that the alloy is located at the boundary between two (Al)/Al₂₇Ca₃Cu₇ primary crystallization areas and concurrently near a ternary eutectic point.

The Al30Cu1.0Ca and Al36Cu1.0Ca alloys were analyzed in order to clarify the primary crystallization area boundaries of another ternary Al₈CaCu₄ compound that is in equilibrium with the aluminum in this system. The microstructure of both alloys contains bright primary crystals (Figure 5a,b) which, according to the spectral analysis (Table 2), has an excess of copper as compared to the Ca-containing phases considered above. The chemical composition of these crystals obtained after slow solidification is somewhat different from that obtained after accelerated solidification. The latter fact can be coupled with the relatively fine structure of the crystals obtained after solidification, which prevents accurate measurements. Thus, according to the data for the slowly solidified alloy, the observed primary crystals correspond perfectly well to the Al₈CaCu₄ phase [25]. One can also note that the slow solidification of the Al36Cu1.0Ca alloy (Figure 5c) also revealed the presence of lone Al₈CaCu₄ phase primary crystals against the background of the eutectic. The latter fact confirms that the alloy is located near the eutectic point.

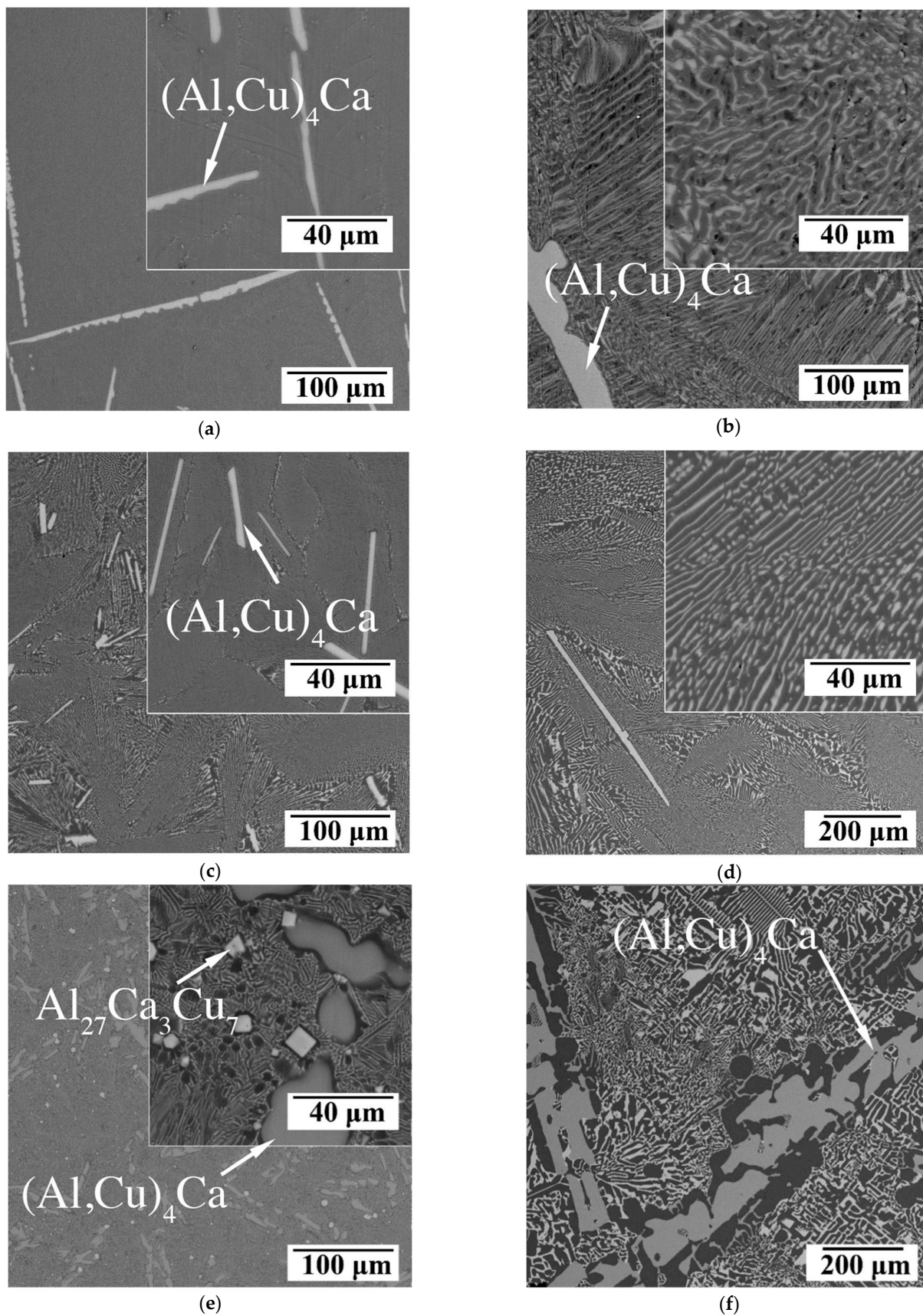


Figure 2. SEM microstructure of the alloys: (a,b) Al1.0Cu8.0Ca, (c,d) Al2.2Cu6.7Ca, (e,f) Al14Cu6.0Ca for cooling rates of (a,c,e) 10 K/s and (b,d,f) 0.02 K/s. (backscattered electron (BSE) images).

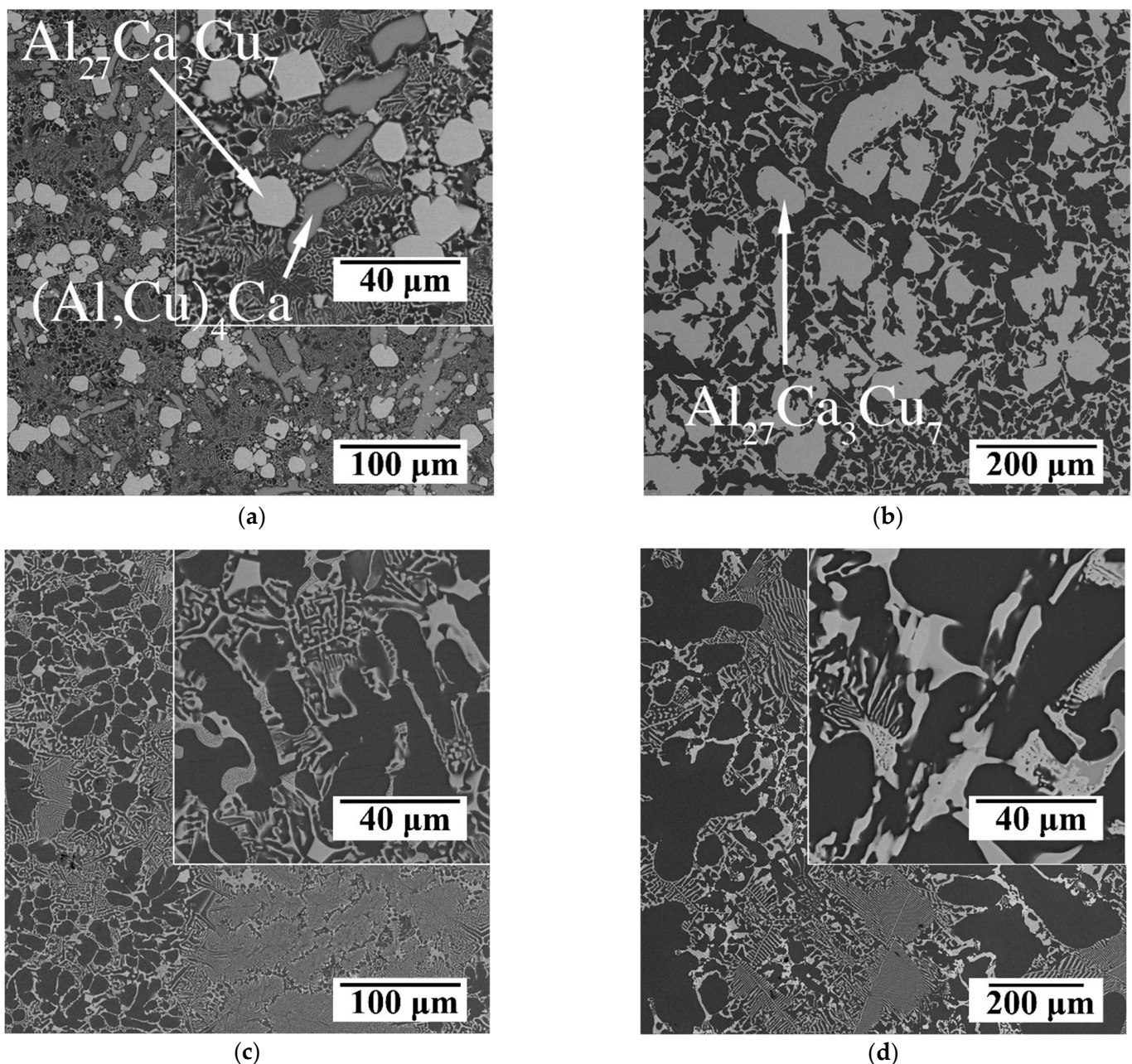


Figure 3. SEM microstructure of the alloys: (a,b) Al18Cu6.0Ca, (c,d) Al14Cu2.5Ca, for cooling rates of (a,c) 10 K/s, and (b,d) 0.02 K/s. BSE.

Finally, the structure of the hypoeutectic alloys with primary aluminum solid solution (Al) crystals was studied. One can see that the Al3.4Cu5.6Ca, Al5.6Cu3.5Ca and Al9.0Cu3.5Ca alloys have a fine hypoeutectic structure (Figure 6). The alloys were also obtained at slow solidification, which coarsens the structural components. The latter fact makes it possible to carry out spectral analysis to determine the chemical composition of crystals. The data (Table 2) suggest that the eutectic in the alloys consists of the (Al,Cu)₄Ca and Al₂₇Ca₃Cu₇ phases. An XRD analysis of the Al5.6Cu3.5Ca alloy (Figure 4) confirmed the presence of these extra phases. Due to the relatively fine structure of the crystals, the measured composition of the Al₂₇Ca₃Cu₇ crystals is somewhat different from the one accepted in [25], but it can still be identified.

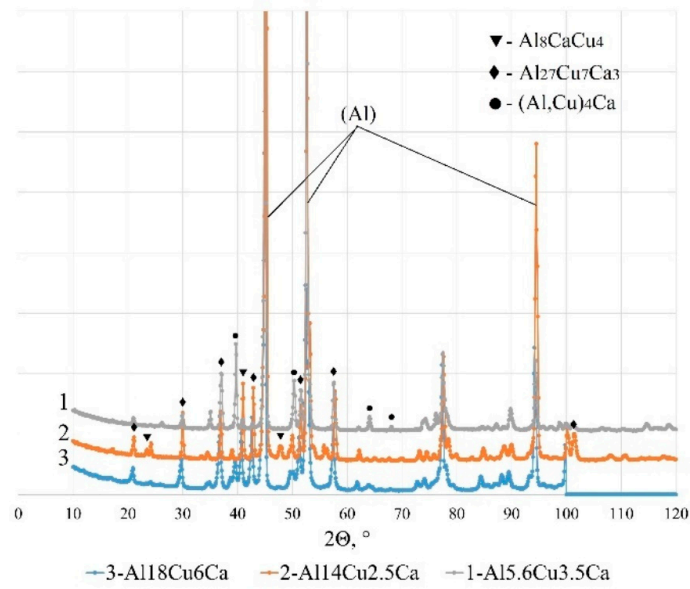


Figure 4. XRD data for (1) Al_{5.6}Cu_{3.5}Ca, (2) Al₁₄Cu_{2.5}Ca and (3) Al₁₈Cu₆Ca alloys. CoK α radiation.

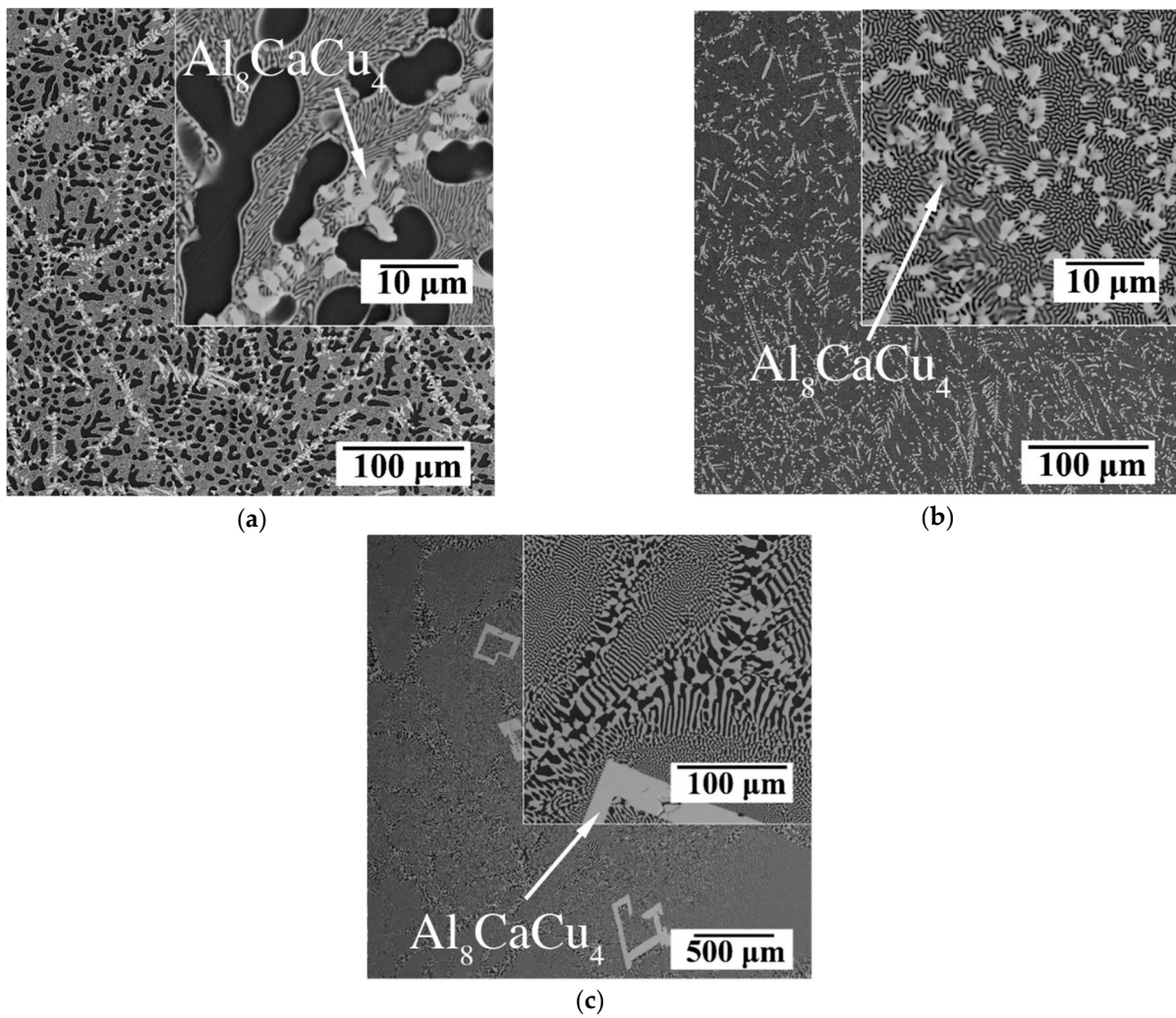


Figure 5. SEM microstructure of the alloys: (a) Al₃₀Cu_{1.0}Ca, and (b,c) Al₃₆Cu_{1.0}Ca for cooling rates of (a,b) 10 K/s, and (c) 0.02 K/s. BSE.

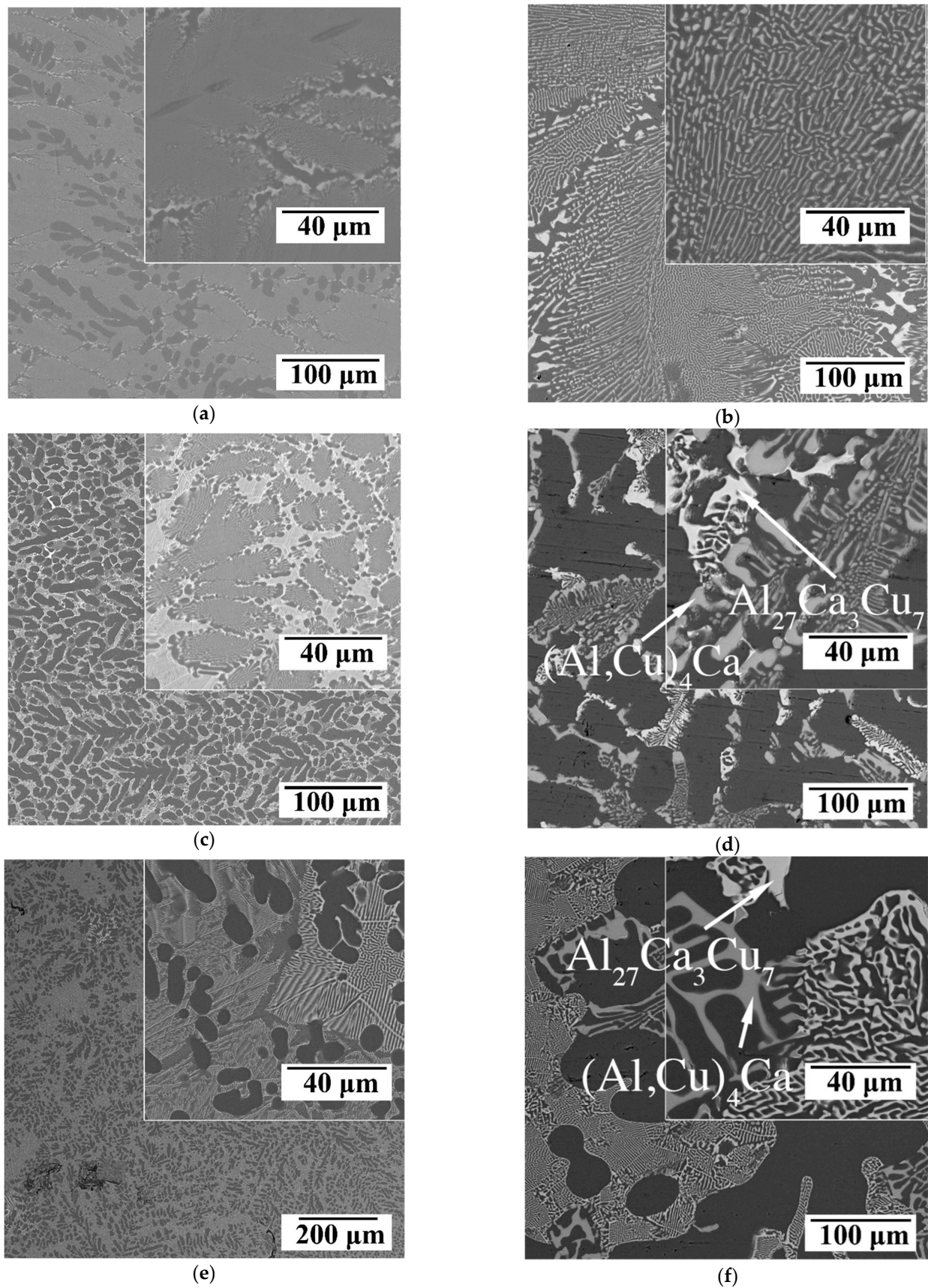


Figure 6. SEM microstructure of the alloys: (a,b) Al_{3.4}Cu_{5.6}Ca, (c,d) Al_{5.6}Cu_{3.5}Ca, (e,f) Al_{9.0}Cu_{3.5}Ca for cooling rates of (a,c,e) 10 K/s and (b,d,f) 0.02 K/s. BSE.

The aforementioned experimental data allow for hypothesizing regarding the boundaries of the primary crystallization areas of the phases considered. It is worthy of note that the analysis did not reveal any traces of peritectic transformations. The structure of the eutectic type diagram is therefore suggested to have two quasi-binary sections: (Al)-Al₂₇Ca₃Cu₇ and (Al)-Al₈CaCu₄ (Figure 7). Indeed, the arrangement of the alloys on the diagram in accordance with the type of primary crystals observed in the structure suggests the existence of three invariant eutectic and two quasi-binary eutectic phase transformations (Table 3). In comparison with another eutectic Al-Ce-Cu system containing one quasi-binary section (Al)-Al₈CeCu₄ and two invariant eutectic transformations (at ~12% Cu, 7% Ce, E1; ~32% Cu, 0.5% Ce, E2) in the aluminum corner, the new Al-Ca-Cu system is preferable for the design of aluminum matrix composites with an excess of eutectic. Indeed, the E1 point in the new Al-Ca-Cu system is located at the copper content typical of industrial alloys, whereas a much higher copper concentration is needed for the Al-Ce-Cu system (~12% Cu for the E1 eutectic point). Moreover, taking into account the very similar content of the third component (7% Ce and 6% Ca) at the E1 point in the systems, the use of cheaper and lighter calcium instead of cerium is preferable. One should note that the estimated position of E3 in Al-Ca-Cu is very close to that of the respective E2 points in the Al-Ce-Cu system. It can therefore be concluded that the position of E3 is calculated with an acceptable accuracy. In comparison with another copper containing ternary system in which the third component has a very limited solubility in aluminum, i.e., Al-Cu-Fe [29], the position of this point is also quite close (~32.5% Cu, 0.3% Fe) to the respective point in the new system.

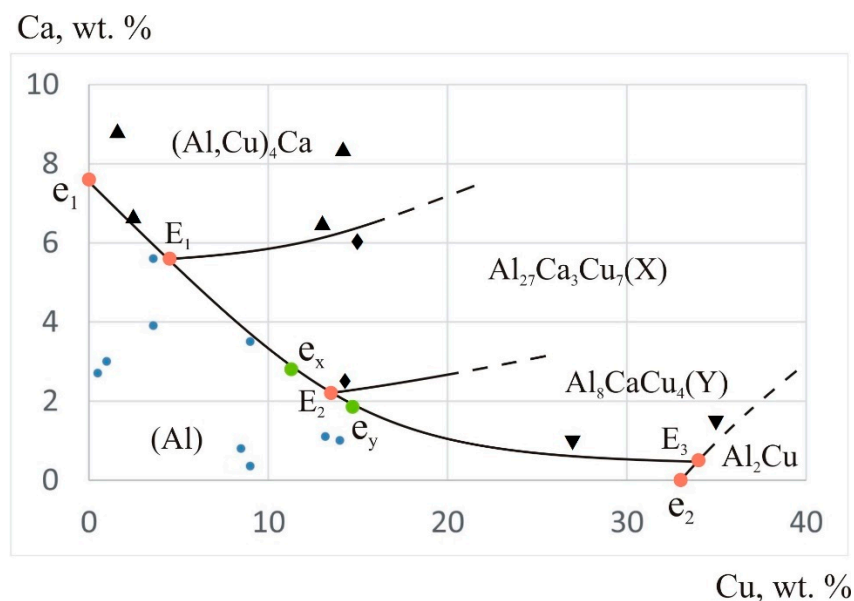


Figure 7. Experimental liquidus projection of the Al-Ca-Cu system in the aluminum corner. The symbols mark the compositions of the alloys for which a specific type of primary crystals is observed.

Table 3. Coordinates of invariant phase transformations.

| Phase Transformation | Point on the Diagram | Chemical Composition, wt.% | | | T, °C |
|---|----------------------|----------------------------|-----|------|-------|
| | | Al | Ca | Cu | |
| L → (Al) + (Al,Cu) ₄ Ca + Al ₂₇ Ca ₃ Cu ₇ | E ₁ | balance | 5.6 | 4.5 | 595 |
| L → (Al) + Al ₂₇ Ca ₃ Cu ₇ + Al ₈ CaCu ₄ | E ₂ | balance | 2.2 | 13.5 | 594 |
| L → (Al) + Al ₈ CaCu ₄ + Al ₂ Cu | E ₃ | balance | 0.5 | 34 | 544 |
| L → (Al) + Al ₂₇ Ca ₃ Cu ₇ | e _x | balance | 2.8 | 11.3 | 596 |
| L → (Al) + Al ₈ CaCu ₄ | e _y | balance | 1.8 | 14.7 | 596 |

To assess the temperature of the invariant phase transformations, some alloys from the corresponding phase fields were subjected to thermal analysis in order to plot their cooling and heating curves (Figure 8). The temperature of invariant transformation is visualized as a platform at a constant temperature. The Al₉Cu_{3.5}Ca and Al₁₄Cu₇Ca alloys were chosen since they pertain to the (Al) + (Al,Cu)₄Ca + Al₂₇Ca₃Cu₇ ternary phase field, and their solidification must end at the temperature of the E1 eutectic transformation. Thermal analysis showed (Figure 8a) that the L → (Al) + (Al,Cu)₄Ca + Al₂₇Ca₃Cu₇ eutectic transformation temperature is about ~595 °C, which is ~22 °C lower than that of the L → (Al) + (Al,Cu)₄Ca eutectic transformation in the binary system [16]. The next two Al₉Cu_{1.5}Ca and Al₁₄Cu_{2.5}Ca alloys pertain to the other ternary phase field, (Al) + Al₂₇Ca₃Cu₇ + Al₈CaCu₄, and their solidification must end at the temperature of the E2 eutectic transformation. An analysis revealed that the latter temperature is also close to 594–595 °C. One should note that since the positions of the eutectic points e_x and e_y in the quasi-binary sections are quite close to the invariant eutectic point E2, the difference in the temperatures should also be negligible. Thus, the temperatures of the e_x and e_y transformations can be assumed to be a few degrees higher than that of E2. Additional precision studies are required for a more accurate determination of these temperatures. One should note that the thermal curves of the Al₁₄Cu_{2.5}Ca alloy contain one more very narrow platform at ~544 °C (marked by arrow in Figure 8b). This transformation is a prime consequence of the elevated solubility of copper in aluminum (to be discussed below) leading to the (L → (Al) + Al₈CaCu₄ + Al₂Cu) ternary eutectic transformation, which is non-equilibrium for this phase field. On the contrary, equilibrium solidification of the last two Al₉Cu_{0.5}Ca and Al₁₄Cu₁Ca alloys must end via this ternary transformation, the temperature of which is about 544 °C (Figure 8c). This temperature is close to that of the L → (Al) + Al₂Cu eutectic transformation in the binary system (548 °C) and the ternary eutectics at the respective points in the Al-Ce-Cu (545 °C) and Al-Ce-Fe (542 °C) systems.

3.2. Isothermal Section at 530 °C

For the Al-Ce-Cu system, the solubility of copper in (Al) reaches 5.7 wt.% in the (Al) + Al₈CeCu₄ + Al₂Cu ternary phase field and 5.7 wt.% in the (Al) + Al₈CeCu₄ quasi-binary section; therefore the alloys from these phase fields can be prone to precipitation hardening. Annealing temperatures in the range of 530–540 °C are commonly used for solid solution treatment before the quenching of the Al-Cu based alloys. Some alloys from the new system were studied after long-term annealing at 530 °C, which is expected to cause the dissolution of most of the nonequilibrium eutectic Al₂Cu phase. An analysis revealed that the copper solubility in (Al) in the (Al) + Al₂₇Ca₃Cu₇ + (Al,Cu)₄Ca ternary phase field is very low and can be accepted as a few tenths of a percent. However, in the rest of the ternary phase field, the copper solubility in (Al) is high enough. Two alloys Al₁₀Cu_{1.5}Ca (Figure 9a) and Al₁₀Cu_{0.5}Ca (Figure 9b) were chosen for the study. The phase composition of the alloys was theoretically assessed based on a simple stoichiometric balance corresponding to the alloy composition. For the hypoeutectic Al₁₀Cu_{1.5}Ca alloy from the (Al) + Al₂₇Ca₃Cu₇ + Al₈CaCu₄ ternary phase field (Table 4), an EMPA analysis of the aluminum matrix showed a copper solubility of up to ~2.4 wt.%. For the Al₁₀Cu_{0.5}Ca alloy pertaining to another ternary phase field (Al) + Al₈CaCu₄ + Al₂Cu (Table 4), the copper solubility is approximately at the solubility limit, i.e., ~5.1 wt.%, which is close to that for the binary Al-Cu and ternary Al-Ce-Cu systems at the same temperature. Thus, the alloys pertaining to the (Al) + Al₈CaCu₄ quasi-binary section and the (Al) + Al₈CaCu₄ + Al₂Cu ternary phase field can also be prone to precipitation hardening. However, for a noticeable precipitation hardening response, the content of copper in the alloy should be about ten times the calcium content. The latter fact makes the precipitation hardening of the Al-Ca-Cu ternary alloy less interesting due to the high content of expensive and heavy copper. However, the transition to more complex systems containing Al-Ca-Cu can help to solve this issue by rearranging the distribution of copper between the aluminum and eutectic phases. The obtained isothermal section of the system at 530 °C is presented in Figure 10.

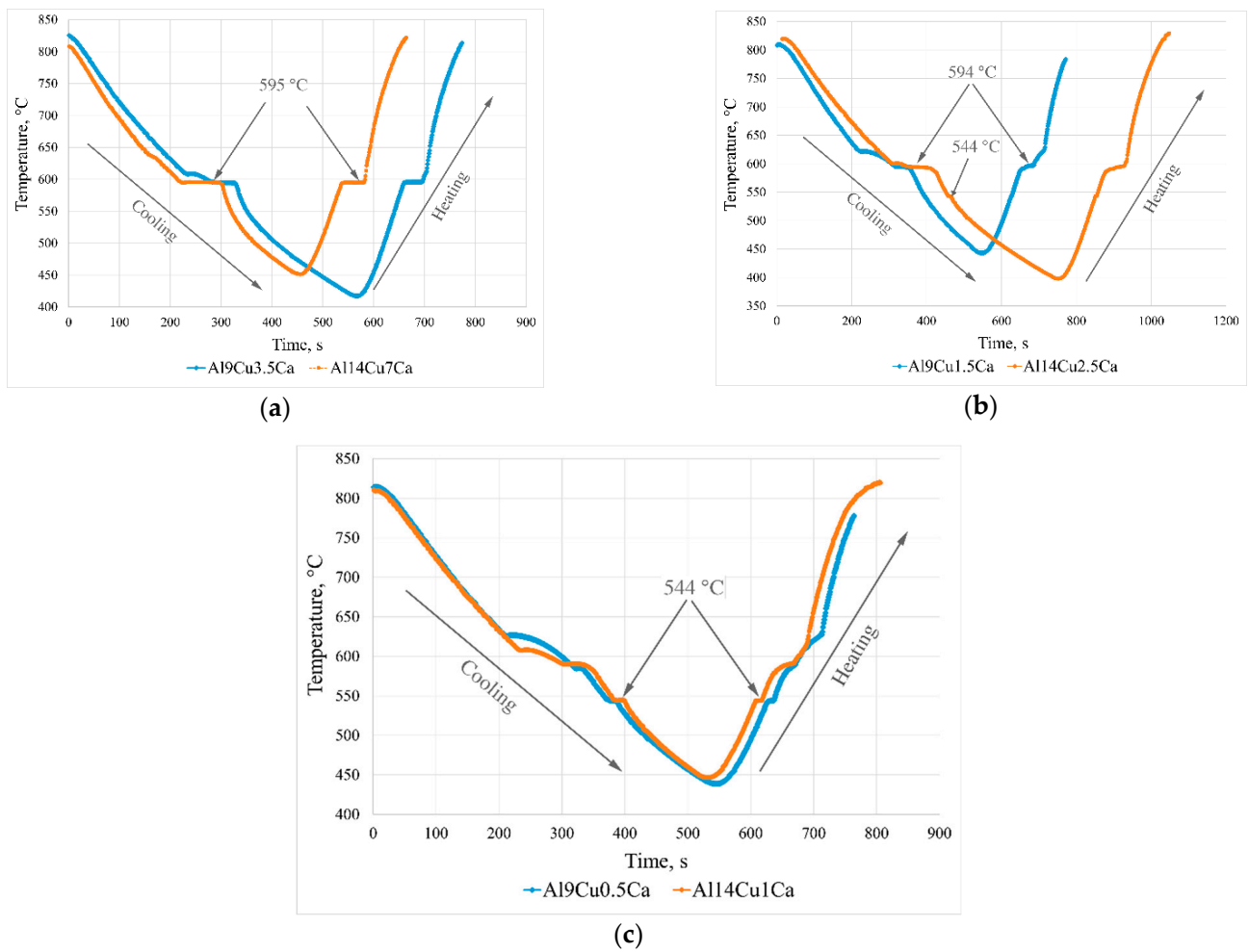


Figure 8. DTA for the alloys: (a) Al9Cu3.5Ca and Al14Cu7Ca, (b) Al9Cu1.5Ca and Al14Cu2.5Ca, (c) Al9Cu0.5Ca and Al14Cu1Ca.

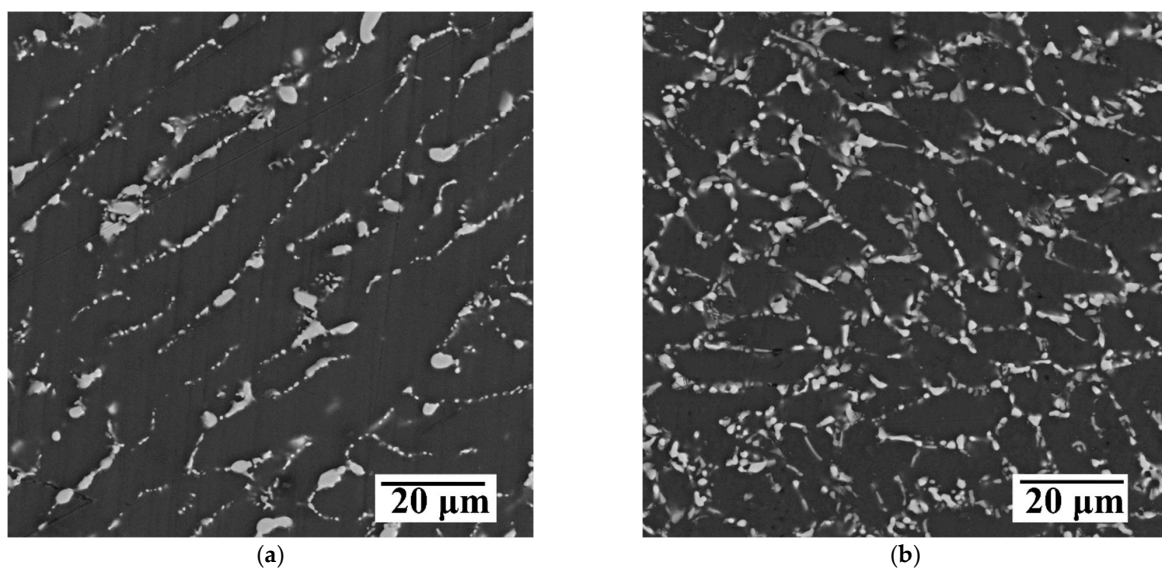


Figure 9. SEM microstructure of the alloys: (a) Al10Cu0.5Ca and (b) Al10Cu1.5Ca after homogenization annealing at 530 °C for 12 h.

Table 4. The measured chemical composition of the aluminum matrix (Al) after homogenization and calculated fractions of extra phases.

| Alloy | Chemical Composition, wt.% | | | Fractions of Extra Phases, wt.% (vol.%) | | |
|-------------|----------------------------|-----------|----|---|--------------------|--|
| | Al | Cu | Ca | Al ₈ CaCu ₄ | Al ₂ Cu | Al ₂₇ Ca ₃ Cu ₇ |
| Al10Cu0.5Ca | balance | 5.1 ± 0.2 | - | 6.2 (3.9) | 3.3 (2.2) | - |
| Al10Cu1.5Ca | balance | 2.4 ± 0.2 | - | 11.0 (7.0) | - | 6.9 (5.7) |

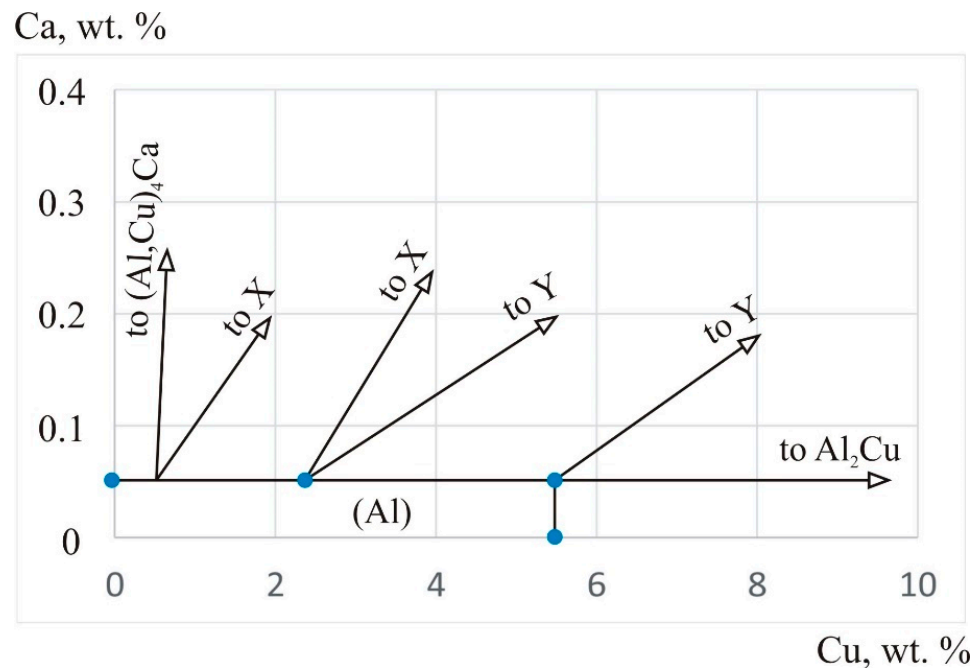


Figure 10. Isothermal section of the Al-Ca-Cu system in the Al-rich corner at 530 °C. X is the Al₂₇Ca₃Cu₇ phase and Y is the Al₈CaCu₄ phase.

3.3. Alloy Examples

The prospects of this system for designing new eutectic type alloys with a natural composite structure are demonstrated for the example of the Al₃Ca0.5Cu and Al₃Ca1Cu alloys. Indeed, as one can see from Figure 11, both alloys are hypoeutectic (Figure 11a,c) and have an ultra-fine eutectic component. Both alloys are near the boundary between the (Al) + (Al,Cu)₄Ca / (Al) + (Al,Cu)₄Ca + Al₂₇Ca₃Cu₇ phase fields with a predominant eutectic (Al,Cu)₄Ca phase. The alloys without preliminary annealing were subjected to hot rolling at a moderate temperature of 300 °C to 2 mm sheets (a total deformation degree of 80%). A microscopic analysis (Figure 11b,d) did not reveal any significant refinement of the structure upon deformation processing. Indeed, the as-cast eutectic colonies are still well resolved, but they are elongated in the rolling direction. The slight differences from the as-cast structure are due to the relatively low degree of deformation.

The hardness of both alloys after rolling is about the same, ~60 Hv. The obtained hot rolled sheets were also subjected to uniaxial tensile tests. The data on the mechanical properties are presented in Figure 12. The obtained level of mechanical properties is moderate yet acceptable for base model alloys. Indeed, in comparing these alloys with the closest counterparts containing a similar [30] or a higher [31] amount of calcium but more expensive rare earth metals (UTS 240–260 MPa, YS 85–205 MPa and δ 5.5–9.0%) [30,31] and nickel (UTS ~190–303 MPa, YS ~150–220 MPa and δ ~0.5–5%) [31] instead of copper, one can see similar mechanical properties, while the latter alloys contain additional hardening additives. One should also note that due to both the eutectic-type structure of the system and the presence of a high amount of numerous insoluble aluminides, the new system

and the alloys may be promising for additive manufacturing techniques such as selective laser melting.

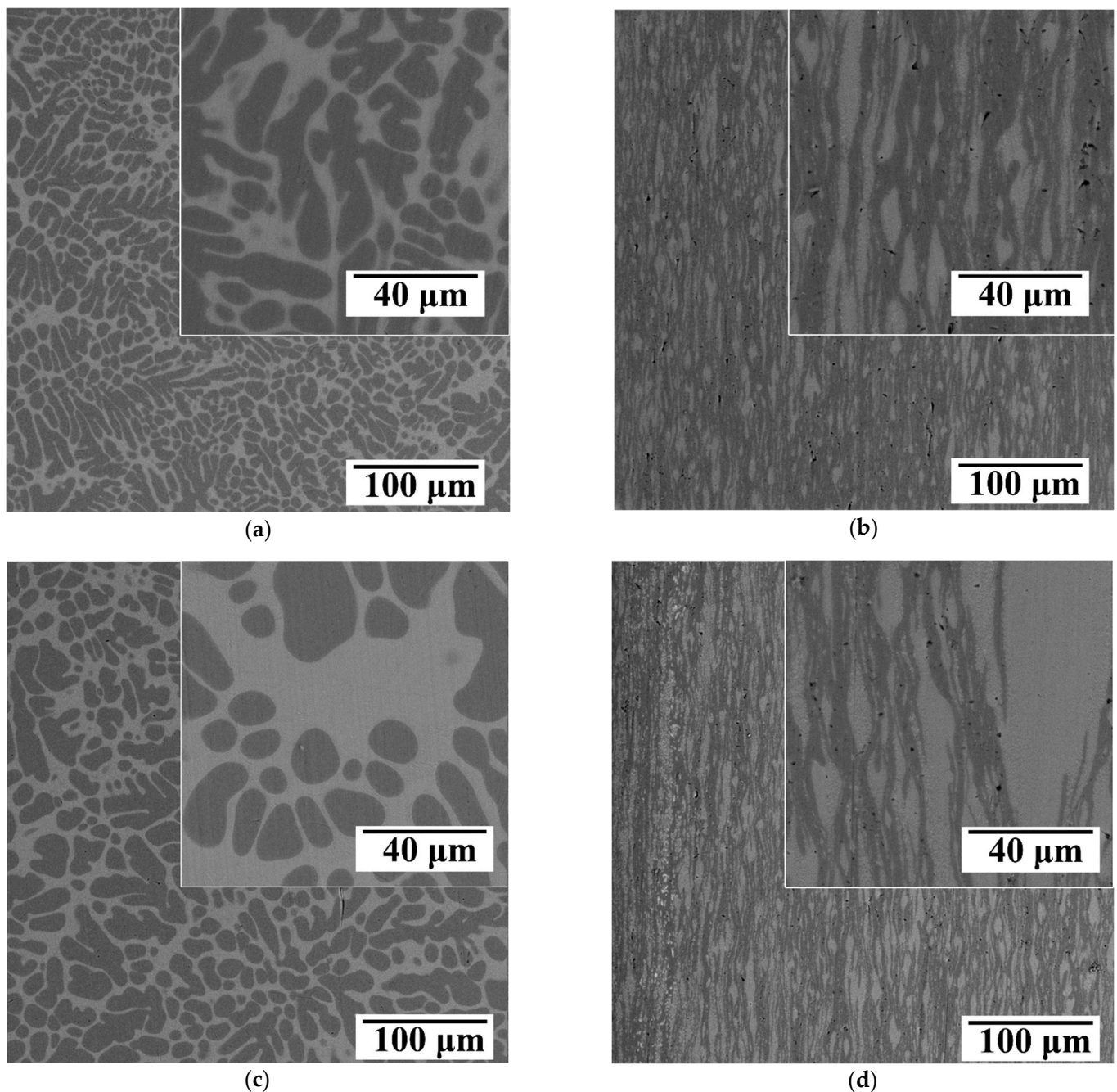


Figure 11. SEM microstructure of the alloys: (a,b) Al₃Ca_{0.5}Cu, (c,d) Al₃Ca₁Cu, (a,c) as-cast, (b,d) hot rolled at 300 °C.

One should also note that a slight increase in the copper content from 0.5 to 1.0 wt.% leads to a minor increase in the strength and a much greater increase in the ductility. The origins of the latter fact are not clear, and more detailed studies are required to determine the causes underlying this phenomenon. It is possible that this can be associated with an expectable increase in the fraction of the Al₂₇Ca₃Cu₇ phase, leading to a modification of the eutectic or an increase in the solubility of copper in the (Al,Cu)₄Ca phase, leading to a change in the properties of the (Al,Cu)₄Ca compound.

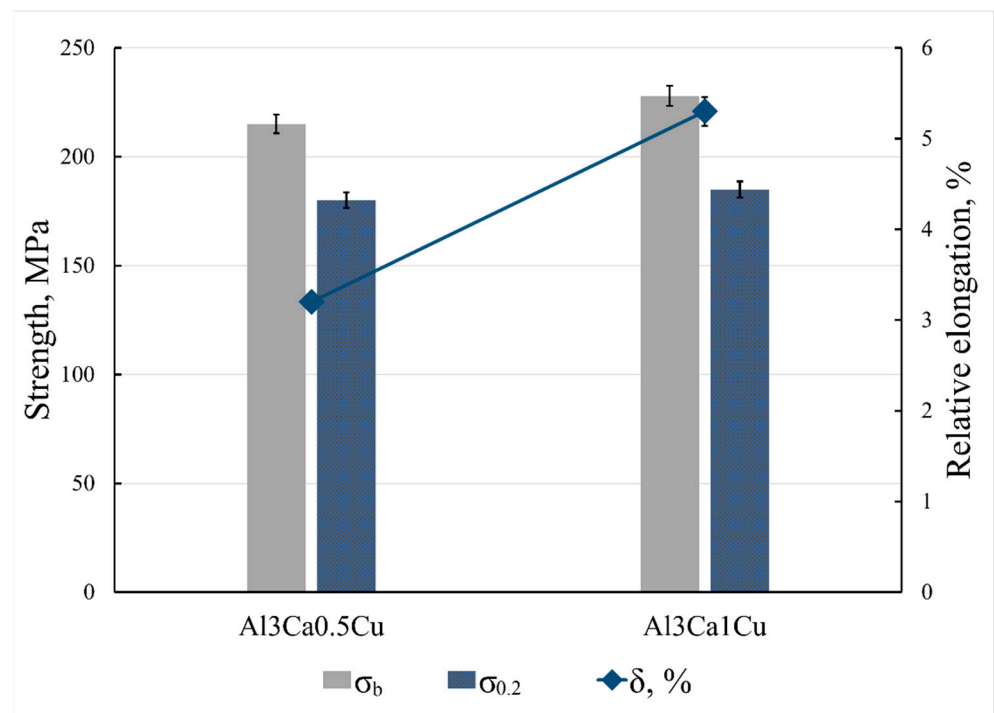


Figure 12. Mechanical properties of the Al3Ca0.5Cu and Al3Ca1Cu sheet alloys.

4. Summary

- (1) The liquidus projection of the Al-Ca-Cu system in the aluminum corner was suggested based on experiential studies of the microstructure and phase composition of model alloys. The suggested structure of the diagram has two quasi-binary sections: (Al)-Al₂₇Ca₃Cu₇ and (Al)-Al₈CaCu₄, and three invariant ternary eutectic transformations: L→(Al) + (Al,Cu)₄Ca + Al₂₇Ca₃Cu₇ (at 5.6 wt.% Ca, 4.5 wt.% Cu, 595 °C), L→(Al) + Al₂₇Ca₃Cu₇ + Al₈CaCu₄ (at 2.2 wt.% Ca, 13.5 wt.% Cu, 594 °C) and L→(Al) + Al₈CaCu₄ + Al₂Cu (at 0.5 wt.% Ca, 34 wt.% Cu, 544 °C). The eutectic point in the quasi-binary sections is accepted to be as follows: L→(Al) + Al₂₇Ca₃Cu₇ (at 2.8 wt.% Ca, 11.3 wt.% Cu) and L→(Al) + Al₈CaCu₄ (at 1.8 wt.% Ca, 14.7 wt.% Cu).
- (2) A study of the copper solubility limit in (Al) revealed that the copper solubility in the (Al) + Al₂₇Ca₃Cu₇ + (Al,Cu)₄Ca ternary phase field is small and can be accepted as a few tenths of a percent. In the (Al)+Al₂₇Ca₃Cu₇+ Al₈CaCu₄ ternary phase field, the copper solubility reaches ~2.4 wt.%, while in the other ternary phase field, (Al) + Al₈CaCu₄ + Al₂Cu is close to the solubility limit, i.e., ~5.1 wt.%, which is close to that for the binary Al-Cu and the ternary Al-Ce-Cu systems. Thus, the alloys pertaining to the (Al) + Al₈CaCu₄ quasi-binary section and the (Al) + Al₈CaCu₄ + Al₂Cu ternary phase field can be prone to precipitation hardening.
- (3) The prospects of this system for designing new eutectic type alloys with a natural composite structure were demonstrated for the example of the Al3Ca0.5Cu and Al3Ca1Cu alloys. The alloys have an ultra-fine eutectic structure based on the (Al,Cu)₄Ca eutectic phase. The alloys showed high manufacturability for moderate temperature hot rolling (300 °C). Uniaxial tensile tests carried out for the obtained 2 mm sheet alloys revealed the following mechanical properties: UTS up to 220 MPa, YS up to 180 MPa, and relative elongation up to 5.5%, which are acceptable for the model alloys.

Author Contributions: Conceptualization, T.K.A. and N.A.B.; Data curation, S.O.C. and X.D.N.; Investigation, N.V.L., S.O.C. and X.D.N.; Methodology, T.K.A. and N.V.L.; Writing—original draft, T.K.A.; Writing—review and editing, T.K.A. and N.A.B. All authors have read and agreed to the published version of the manuscript.

Funding: This work was financially supported by the Moscow Polytechnic University within the framework of the grant named after Pyotr Kapitsa.

Data Availability Statement: The raw/processed data required to reproduce these findings cannot be shared at this time due to technical or time limitations.

Acknowledgments: The authors would like to thank Tatyana Sviridova (The National University of Science and Technology MISiS) for conducting the X-ray phase analysis.

Conflicts of Interest: The authors declare that they have no conflict of interest.

References

1. Polmear, I.J.; Couper, M.J. Design and development of an experimental wrought aluminum alloy for use at elevated temperatures. *Metall. Trans. A* **1988**, *19*, 1027–1035. [\[CrossRef\]](#)
2. Mondol, S.; Kashyap, S.; Kumar, S.; Chattopadhyay, K. Improvement of high temperature strength of 2219 alloy by Sc and Zr addition through a novel three-stage heat treatment route. *Mater. Sci. Eng. A* **2018**, *732*, 157–166. [\[CrossRef\]](#)
3. Bourgeois, L.; Dwyer, C.; Weyland, M.; Nie, J.; Muddle, B.C. Structure and energetics of the coherent interface between the θ' precipitate phase and aluminium in Al–Cu. *Acta Mater.* **2011**, *59*, 7043–7050. [\[CrossRef\]](#)
4. Ding, H.; Fu, H.Z.; Liu, Z.Y.; Chen, R.Z.; Liu, B.C. Compensation of solidification contraction and hot cracks tendency of alloy. *Acta Metall. Sin.* **1997**, *33*, 921–926.
5. Sims, Z.C.; Weiss, D.; McCall, S.K.; McGuire, M.A.; Ott, R.T.; Geer, T.; Rios, O.; Turchi, P.A.E. Cerium-based, intermetallic-strengthened aluminum casting alloy: High-volume co-product development. *JOM* **2016**, *68*, 1940–1947. [\[CrossRef\]](#)
6. Belov, N.A.; Khvan, A.V.; Alabin, A.N. Microstructure and phase composition of Al–Ce–Cu alloys in the Al-rich corner. *Mater. Sci. Forum* **2006**, *519–521*, 395–400. [\[CrossRef\]](#)
7. Li, M.; Wang, H.; Wei, Z.; Zhu, Z. The effect of Y on the hot-tearing resistance of Al–5 wt.% Cu based alloy. *Mater. Des.* **2010**, *31*, 2483–2487. [\[CrossRef\]](#)
8. Belov, N.A.; Khvan, A.V. The ternary Al–Ce–Cu phase diagram in the aluminum-rich corner. *Acta Mater.* **2007**, *55*, 5473–5482. [\[CrossRef\]](#)
9. Pozdniakov, A.V.; Barkov, R.Y.; Amer, S.M.; Levchenko, V.S.; Kotov, A.D.; Mikhaylovskaya, A.V. Microstructure, mechanical properties and superplasticity of the Al–Cu–Y–Zr alloy. *Mater. Sci. Eng. A* **2019**, *758*, 28–35. [\[CrossRef\]](#)
10. Manca, D.R.; Churyumov, A.Y.; Pozdniakov, A.V.; Prosviryakov, A.S.; Ryabov, D.K.; Krokhin, A.Y.; Korolev, V.A.; Daubarayte, D.K. Microstructure and Properties of Novel Heat Resistant Al–Ce–Cu Alloy for Additive Manufacturing. *Met. Mater. Int.* **2019**, *25*, 633–640. [\[CrossRef\]](#)
11. Shurkin, P.; Akopyan, T.; Korotkova, N.; Prosviryakov, A.; Bazlov, A.; Komissarov, A.; Moskovskikh, D. Microstructure and Hardness Evolution of Al₈Zn₇Ni₃Mg Alloy after Casting at very Different Cooling Rates. *Metals* **2020**, *10*, 762–776. [\[CrossRef\]](#)
12. Chen, B.; Moon, S.K.; Yao, X.; Bi, G.; Shen, J.; Umeda, J.; Kondoh, K. Strength and strain hardening of a selective laser melted AlSi10Mg alloy. *Scripta Mater.* **2017**, *141*, 45–49. [\[CrossRef\]](#)
13. Delahaye, J.; Tchuindjang, J.T.; Lecomte-Beckers, J.; Rigo, O.; Habraken, A.M.; Mertens, A. Influence of Si precipitates on fracture mechanisms of AlSi10Mg parts processed by Selective Laser Melting. *Acta Mater.* **2019**, *175*, 160–170. [\[CrossRef\]](#)
14. Bahl, S.; Plotkowski, A.; Sisco, K.; Leonard, D.N.; Allard, L.F.; Michi, R.A.; Poplawsky, J.D.; Dehoff, R.; Shyam, A. Elevated temperature ductility dip in an additively manufactured Al–Cu–Ce alloy. *Acta Mater.* **2021**, *220*, 117285. [\[CrossRef\]](#)
15. Bahl, S.; Sisco, K.; Yang, Y.; Theska, F.; Primig, S.; Allard, L.F.; Michi, R.A.; Fancher, C.; Stump, B.; Dehoff, R.; et al. Al–Cu–Ce–(Zr) alloys with an exceptional combination of additive processability and mechanical properties. *Addit. Manuf.* **2021**, *48*, 102404. [\[CrossRef\]](#)
16. Mondolfo, L.F. *Aluminium Alloys: Structure and Properties*, 1st ed.; Butterworths: London, UK, 1976; pp. 29–30.
17. Akopyan, T.K.; Belov, N.A.; Lukyanchuk, A.A.; Letyagin, N.V.; Sviridova, T.A.; Petrova, A.N.; Fortuna, A.S.; Musin, A.F. Effect of high pressure torsion on the precipitation hardening in Al–Ca–La based eutectic alloy. *Mater. Sci. Eng. A* **2021**, *802*, 140633. [\[CrossRef\]](#)
18. Akopyan, T.K.; Letyagin, N.V.; Sviridova, T.A.; Korotkova, N.O.; Prosviryakov, A.S. New Casting Alloys Based on the Al+Al₄(Ca,La) Eutectic. *JOM* **2020**, *72*, 3779–3786. [\[CrossRef\]](#)
19. Belov, N.A.; Naumova, E.A.; Akopyan, T.K.; Doroshenko, V.V. Design of multicomponent aluminium alloy containing 2 wt.% Ca and 0.1 wt.% Sc for cast products. *J. Alloys Compd.* **2018**, *762*, 528–536. [\[CrossRef\]](#)
20. Belov, N.A.; Naumova, E.A.; Akopyan, T.K.; Doroshenko, V.V. Phase Diagram of Al–Ca–Mg–Si System and Its Application for the Design of Aluminum Alloys with High Magnesium Content. *Metals* **2017**, *7*, 429. [\[CrossRef\]](#)
21. Gamin, Y.V.; Belov, N.A.; Akopyan, T.K.; Timofeev, V.N.; Cherkasov, S.O.; Motkov, M.M. Effect of Radial-Shear Rolling on the Structure and Hardening of an Al–8%Zn–3.3%Mg–0.8%Ca–1.1%Fe Alloy Manufactured by Electromagnetic Casting. *Materials* **2023**, *16*, 677. [\[CrossRef\]](#) [\[PubMed\]](#)
22. Belov, N.; Akopyan, T.; Korotkova, N.; Murashkin, M.; Timofeev, V.; Fortuna, A. Structure and Properties of Ca and Zr Containing Heat Resistant Wire Aluminum Alloy Manufactured by Electromagnetic Casting. *Metals* **2021**, *11*, 236. [\[CrossRef\]](#)

23. Letyagin, N.V.; Shurkin, P.K.; Nguen, Z.; Koshmin, A.N. Effect of Thermodeformation Treatment on the Structure and Mechanical Properties of the Al₃Ca₁Cu_{1.5}Mn Alloy. *Phys. Met. Metallogr.* **2021**, *122*, 814–819. [[CrossRef](#)]
24. Letyagin, N.V.; Musin, A.F.; Sichev, L.S. New aluminum-calcium casting alloys based on secondary raw materials. *Mater. Today Proc.* **2021**, *38*, 1551–1555. [[CrossRef](#)]
25. Akopyan, T.K.; Sviridova, T.A.; Belov, N.A.; Letyagin, N.V.; Korotitskiy, A.V. Description of intermetallic compounds in equilibrium with aluminum in the new Al–Ca–Cu ternary alloying system. *Trans. Nonferrous Met. Soc. China* **2023**.
26. Bo, H.; Jin, S.; Zhang, L.G.; Chen, X.M.; Chen, H.M.; Liu, L.B.; Zheng, F.; Jin, Z.P. Thermodynamic assessment of Al–Ce–Cu system. *J. Alloys Compd.* **2009**, *484*, 286–295. [[CrossRef](#)]
27. Shelekhov, E.V.; Sviridova, T.A. Programs for X-ray analysis of polycrystalline. *Met. Sci. Heat Treat.* **2000**, *42*, 309. [[CrossRef](#)]
28. Andersson, J.O.; Helander, T.; Höglund, L.; Shi, P.; Sundman, B. Thermo-Calc and DICTRA, Computational Tools for Materials Science. *Calphad* **2002**, *26*, 273–312. [[CrossRef](#)]
29. Glazoff, M.V.; Khvan, A.; Zolotarevsky, V.S.; Belov, N.A. *Casting Aluminum Alloys: Their Physical and Mechanical Metallurgy*, 2nd ed.; Elsevier: London, UK, 2010; pp. 52–53.
30. Letyagin, N.V.; Akopyan, T.K.; Nguen, Z.; Sviridova, T.A.; Koshmin, A.N.; Aksenov, A.A. The effect of La on the microstructure and mechanical properties of the (Al) + Al₄(Ca,La) wrought alloys. *Phys. Met. Metallogr.* **2023**, *124*, 80–86.
31. Naumova, E.A.; Akopyan, T.K.; Letyagin, N.V.; Vasina, M.A. Investigation of the structure and properties of eutectic alloys of the Al–Ca–Ni system containing REM. *Non-Ferr. Met.* **2018**, *2*, 29–36. [[CrossRef](#)]

Disclaimer/Publisher’s Note: The statements, opinions and data contained in all publications are solely those of the individual author(s) and contributor(s) and not of MDPI and/or the editor(s). MDPI and/or the editor(s) disclaim responsibility for any injury to people or property resulting from any ideas, methods, instructions or products referred to in the content.